

Classification of aeroacoustically relevant surface modes in cylindrical lined ducts

E. J. Brambley, N. Peake

*Department of Applied Mathematics and Theoretical Physics, University of Cambridge,
Centre for Mathematical Sciences, Wilberforce Road, Cambridge CB3 0WA, UK*

Published in Wave Motion **43** (2006) 301–310.

Submitted 11 November 2005; submitted in revised form 30 November 2005; accepted 13 January 2006.

© 2006 Elsevier B.V. All rights reserved.

Abstract

Wave modes in a straight cylindrical duct with a locally-reacting boundary and a steady subsonic axial flow are investigated. The duct modes are separated into ordinary duct modes and surface modes confined to a neighbourhood of the boundary. Previous asymptotic results of Rienstra for the surface modes assume that the dimensionless frequency ω is large, and that the azimuthal order $m \ll \omega$. In this paper, these results are generalized to arbitrary values of m , as applicable to rotor-alone noise in aeroengines where m is a multiple of the number of blades and is typically $O(\omega)$. A dimensionless number λ is found to govern the surface modes' behaviour, and qualitatively different behaviour is seen for λ in four distinct regions, separated by critical values depending only on the steady flow Mach number. For aeroacoustically relevant parameters, our generalized asymptotics are shown to provide a distinctly better approximation to the full equations than previous approximations.

1 Introduction

Acoustic waves in a straight circular rigid duct are well understood, with the familiar solution in terms of Bessel's functions of the first kind. If the duct boundary is not rigid but is allowed to oscillate with the flow (for example as a model of an acoustic lining in aeroengines), the dispersion relation becomes more complicated. In this case Rienstra [1] noted that for high frequencies the duct modes can be classified into acoustic modes and surface modes, the latter being localized about the duct boundary, and gave an asymptotically valid dispersion relation for the surface modes in the *high-frequency* limit. Formally, [1] considered the limit $\omega \rightarrow \infty$ for modes of the form $f(r) \exp\{i\omega t - ikx - im\theta\}$ with the azimuthal wavenumber m fixed, where the duct cross-section is described in polar coordinates r and θ with x in the axial direction. A good agreement between the asymptotic and exact results was demonstrated even for modest values of ω , but provided $m \lesssim \omega$.

In this paper, the asymptotic regime $\omega \rightarrow \infty$ is again investigated, but now with $\Omega = \omega/m$ fixed. For the rotor-alone noise produced in an aeroengine, m is an integer multiple of the number of fan blades, while Ω is the rotation rate of the engine (with the nondimensionalization introduced below, Ω becomes the blade-tip Mach number); in this case our asymptotic limit corresponds to a *many-bladed* limit. It turns out that the surface-mode dispersion relation of [1] is recovered from our asymptotic regime in the limit $\Omega \rightarrow \infty$, and thus the results presented here are a generalization of [1] to arbitrary azimuthal order m .

The behaviour of the surface modes is found to be dictated by the value of the nondimensional number $\lambda = \omega r_0 / (m\sqrt{C^2 - U^2})$, where r_0 is the duct radius, U is the axial steady flow speed, and C is the speed of sound. Qualitatively different behaviour is seen for λ in the four regions $0-\lambda_n$, $\lambda_n-\lambda_p$, λ_p-1 , and $1-\infty$, where the critical values λ_n and λ_p correspond to a change in behaviour of the number and position of the surface modes respectively, and are functions of the steady flow Mach number only. The case $\lambda = \infty$ corresponds to the results of [1]. McAlpine & Wright [2] considered the dominant component of noise in an aeroengine intake at high power (with supersonic fan blade-tips) to be the rotor-alone

BPF fundamental mode. The parameters they suggest as being representative of a typical aeroengine correspond to $\lambda \approx 1.5$, for which the surface-mode asymptotics derived here provide a distinctly better approximation to the exact solution than the previous approximation of [1].

2 Governing equations and the dispersion relation

A straight cylindrical duct of radius r_0 and of infinite extent in the x direction is considered. Its cross-section is described by polar coordinates r and θ . A steady uniform axial flow of speed U , density D , and pressure P flows down the inside of the duct in the positive x direction. The fluid is considered to be inviscid and homentropic, with ratio of specific heats γ .

All parameters are nondimensionalized in the standard way to simplify the notation. Speeds are nondimensionalized by the speed of sound $C = (\gamma P/D)^{1/2}$, so that U becomes the steady flow Mach number, from now on considered subsonic. Distances are nondimensionalized by the duct radius r_0 , time by r_0/C , densities by D , and pressure by DC^2 .

A small potential perturbation $\phi(x, r, \theta, t)$ is considered to the steady state, with corresponding velocity perturbation $\nabla\phi$, pressure p and density ρ . The linearized governing equations given by Goldstein [3] in this case become

$$\frac{D^2\phi}{Dt^2} - \nabla^2\phi = 0 \quad \text{and} \quad p = \rho = -\frac{D\phi}{Dt}, \quad (1)$$

where $D/Dt = \partial/\partial t + U\partial/\partial x$ is the convective derivative with respect to the base flow.

In the limit of vanishing viscosity, the boundary layer along the wall reduces to a vortex sheet. The appropriate boundary condition (following [1]) is that of a locally-reacting flexible impermeable surface, for which a time-harmonic forcing $p \exp\{i\omega t - ikx - im\theta\}$ yields an outward wall velocity $v \exp\{\dots\}$. The ratio p/v is termed the impedance Z . Myers [4] derived the linearized boundary condition for a general geometry, which for a straight cylindrical duct with uniform steady flow reduces to

$$i\omega \frac{\partial\phi}{\partial r} = \left(i\omega + U \frac{\partial}{\partial x} \right) \frac{p}{Z}, \quad (2)$$

evaluated on the unperturbed boundary.

2.1 Exact solution in terms of Bessel's functions

A solution to (1) of the form $\phi = f(r) \exp\{i\omega t - ikx - im\theta\}$ is sought. With the nondimensionalization above, ω is the Helmholtz number, k is the *axial wavenumber*, and m (an integer) is the *azimuthal wavenumber*. Substituting this into (1), the radial equation for $f(r)$ is found to be

$$r^2 \frac{d^2 f}{dr^2} + r \frac{df}{dr} + (\alpha^2 r^2 - m^2) f = 0, \quad \text{where} \quad \alpha^2 = (\omega - Uk)^2 - k^2. \quad (3)$$

This is Bessel's equation, up to a scaling of r . The solution is required to be non-singular at $r = 0$, giving the solution in terms of Bessel's functions of the first kind as $f(r) = AJ_m(\alpha r)$, for some constant amplitude A . The boundary condition (2) then yields the dispersion relation

$$1 - \frac{(\omega - Uk)^2}{i\omega Z} \frac{J_m(\alpha)}{\alpha J'_m(\alpha)} = 0. \quad (4)$$

Following [1], the *reduced axial wavenumber* σ is introduced,

$$\sigma = U + \frac{\beta^2}{\omega} k, \quad \text{giving} \quad \alpha^2 = \frac{\omega^2}{\beta^2} (1 - \sigma^2), \quad (5)$$

where $\beta^2 = 1 - U^2$. This is so as to remove the Doppler effect of the base flow and scale σ to be $O(1)$ irrespective of ω . With this transformation, the dispersion relation (4) becomes

$$1 - \frac{\omega}{iZ\beta^4} (1 - U\sigma)^2 \frac{J_m(\alpha)}{\alpha J'_m(\alpha)} = 0. \quad (6)$$

Note that since $J_m(-r) = (-1)^m J_m(r)$, it does not matter which branch is chosen for α , and no branch cut is necessary.

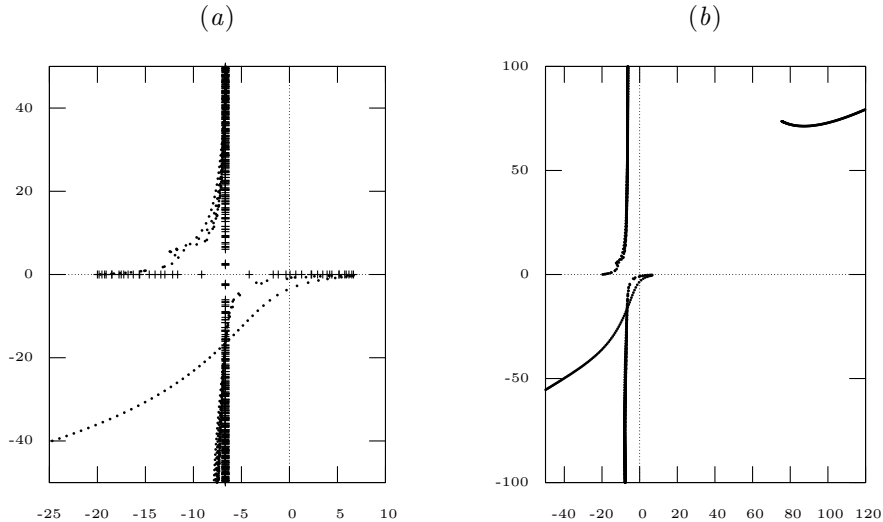


Figure 1: Axial wavenumbers k , for $U = 0.5$, $m = 0, 1, 2, \dots$, $\omega = 10$. (a) Comparison between hard-walled wavenumbers (+) and impedance boundary with $Z = 2 - i$ (o). (b) Larger view showing two surface-mode series, for $Z = 2 - i$.

2.2 Discussion of exact results

For a fixed azimuthal wavenumber m and frequency ω , the dispersion relation (6) yields an infinite discrete set of solutions for σ , and hence for k . The exact solutions are computed numerically using a pseudo-spectral method applied to Bessel's equation (3). In the hard-walled limit $Z \rightarrow \infty$, the dispersion relation (6) simplifies to $J'_m(\alpha) = 0$, with solutions for α along the positive real axis. Fig. 1(a) plots the axial wavenumbers k for a hard-walled duct. It shows a finite number of real wavenumbers corresponding to propagating (*cuton*) modes, and an infinite discrete set of complex wavenumbers corresponding to exponentially decaying (*cutoff*) modes. Also shown are the wavenumbers for an impedance boundary with $Z = 2 - i$. The boundary damping causes all modes to have complex axial wavenumbers and decay in space, although there is still a structure similar to the cuton–cutoff structure of the hard-walled duct. The majority of modes have nearly real radial wavenumbers α , and indeed $\text{Im}(\alpha)$ tends to zero as the modes become more cutoff. However, there are two series of modes, shown in fig. 1(b), for which α has a significant imaginary part. These series, one in the lower left and one in the upper right of the k -plane, contain one mode for each azimuthal wavenumber m . The leading-order asymptotics for Bessel's functions of large complex argument (see e.g. Abramowitz & Stegun [5], p. 364) give

$$\frac{|J_m(\alpha r)|}{|J_m(\alpha)|} \sim r^{-1/2} \exp\{-|\text{Im}(\alpha)|(1-r)\}.$$

Thus, modes for which α has a large imaginary part are confined to within a small distance of the duct boundary, and as in [1] are termed *surface modes*. Other modes for which α is close to the real axis tend to pervade more into the duct, and are termed *acoustic modes*.

3 Surface-mode asymptotics

In this section the dispersion relation (6) is investigated in the limit $\omega \rightarrow \infty$ with m/ω held fixed. From (5) it is expected that $\sigma = O(1)$ and $\alpha = O(\omega)$. This motivates the definitions

$$\omega = m\Omega, \quad \alpha = m\zeta, \quad \lambda = \frac{\Omega}{\beta}, \quad \zeta^2 = \lambda^2(1 - \sigma^2).$$

Note that Ω was used in [1] to represent a different quantity.

The high-frequency limit is obtained by taking $m \rightarrow \infty$ with Ω held fixed. The solutions are expected to be surface waves confined to a thin neighbourhood of the duct boundary, and it turns out the distinguished scaling is obtained by substituting $r = 1 - y/m$ into (3), yielding

$$(m - y)^2 \frac{d^2 f}{dy^2} - (m - y) \frac{df}{dy} + m^2 \left(\zeta^2 \left(1 - \frac{y}{m}\right)^2 - 1 \right) f = 0.$$

To leading order in m , the first and third terms balance, giving

$$\frac{d^2 f}{dy^2} + (\zeta^2 - 1)f = 0,$$

with solution

$$f(y) = e^{-\mu y}, \quad \mu^2 = 1 - \zeta^2, \quad \text{Re}(\mu) > 0.$$

The boundary condition (2) gives the dispersion relation

$$\mu - \frac{\lambda}{iZ\beta^3} (1 - U\sigma)^2 = 0. \quad (7)$$

3.1 Recovery of fixed m asymptotics

The dispersion relation (7) has been obtained by setting $\omega = m\Omega$ and sending $m \rightarrow \infty$ with Ω fixed. The results of [1], for which $\omega \rightarrow \infty$ with m fixed, are recovered from the present analysis in the limit $\Omega \rightarrow \infty$, or equivalently $\lambda \rightarrow \infty$. To see this, first note that the reduced radial wavenumber of [1] is given by $\gamma = \zeta/\lambda$, so that the dispersion relation (7), on division by λ , may be written

$$\left(\frac{1}{\lambda^2} - \gamma^2 \right)^{1/2} - \frac{1}{iZ\beta^3} (1 - U\sigma)^2 = 0.$$

In [1], γ was defined such that $\text{Im}(\gamma) < 0$, while μ is defined so that $\text{Re}(\mu) > 0$. Hence, letting $\lambda \rightarrow \infty$ and multiplying throughout by $-iZ\beta^3$, the dispersion relation becomes

$$(1 - U\sigma)^2 + \beta^3 Z\gamma = 0.$$

This is exactly the result shown in equation 11 of [1]. The asymptotic dispersion relation (7) derived here is thus seen to be a generalization of the surface-mode dispersion relation of [1] to the case of finite λ .

3.2 Number of surface modes

On taking the right hand term of the dispersion relation (7) to the right hand side and squaring both sides, a quartic equation for σ is found,

$$\left(\frac{1}{\lambda^2} - 1 \right) + \sigma^2 + \frac{1}{Z^2\beta^6} (1 - U\sigma)^4 = 0. \quad (8)$$

There are therefore exactly four solutions (counting multiplicity), although some of these solutions may have $\text{Re}(\mu) < 0$ and so must be discounted. A change in the number of valid roots can therefore only occur when one of the roots crosses the line $\text{Re}(\mu) = 0$. This line corresponds to the surface modes becoming acoustic modes, no longer being localized about the duct boundary, and hence the asymptotics above breaking down; in other words, the line $\text{Re}(\mu) = 0$ is an anti-Stokes line. Mapping this anti-Stokes line into the complex Z -plane segregates the Z -plane into regions with different numbers of surface modes.

Fig. 2 shows the anti-Stokes lines mapped into the Z plane for $U = 0.5$. The limit $\lambda = \infty$ corresponds to fig. 5 of [1]. For $1 < \lambda < \infty$ the results of [1] are still qualitatively correct, although quantitatively some variation is seen as λ approaches unity. Specifically, the point (d) approaches positive real infinity as $\lambda \rightarrow 1$. At $\lambda = 1$ a qualitative change is seen, and for $\lambda < 1$ a different regime is entered. As $\tilde{\tau}$ (from table 1) approaches one, the points (b) tend to $\pm i\infty$, and the boundaries of regions I and V approach the imaginary axis. This corresponds to λ approaching $\lambda_n \equiv 1/\sqrt{1 + U^{-2}}$. For $\lambda < \lambda_n$ a third regime is entered in which regions I and V are absent, and as $\lambda \rightarrow 0$ region III expands to fill the whole of the Z -plane. The regions I, II, III, IV, V, VI, and VII contain respectively 0, 1, 2, 3, 4, 1, and 3 surface modes. This explains why there are only two surface-mode series seen in fig. 1(b) for large m , instead of the three predicted by [1] (since $Z = 2 - i$ lies in region III for sufficiently large m).

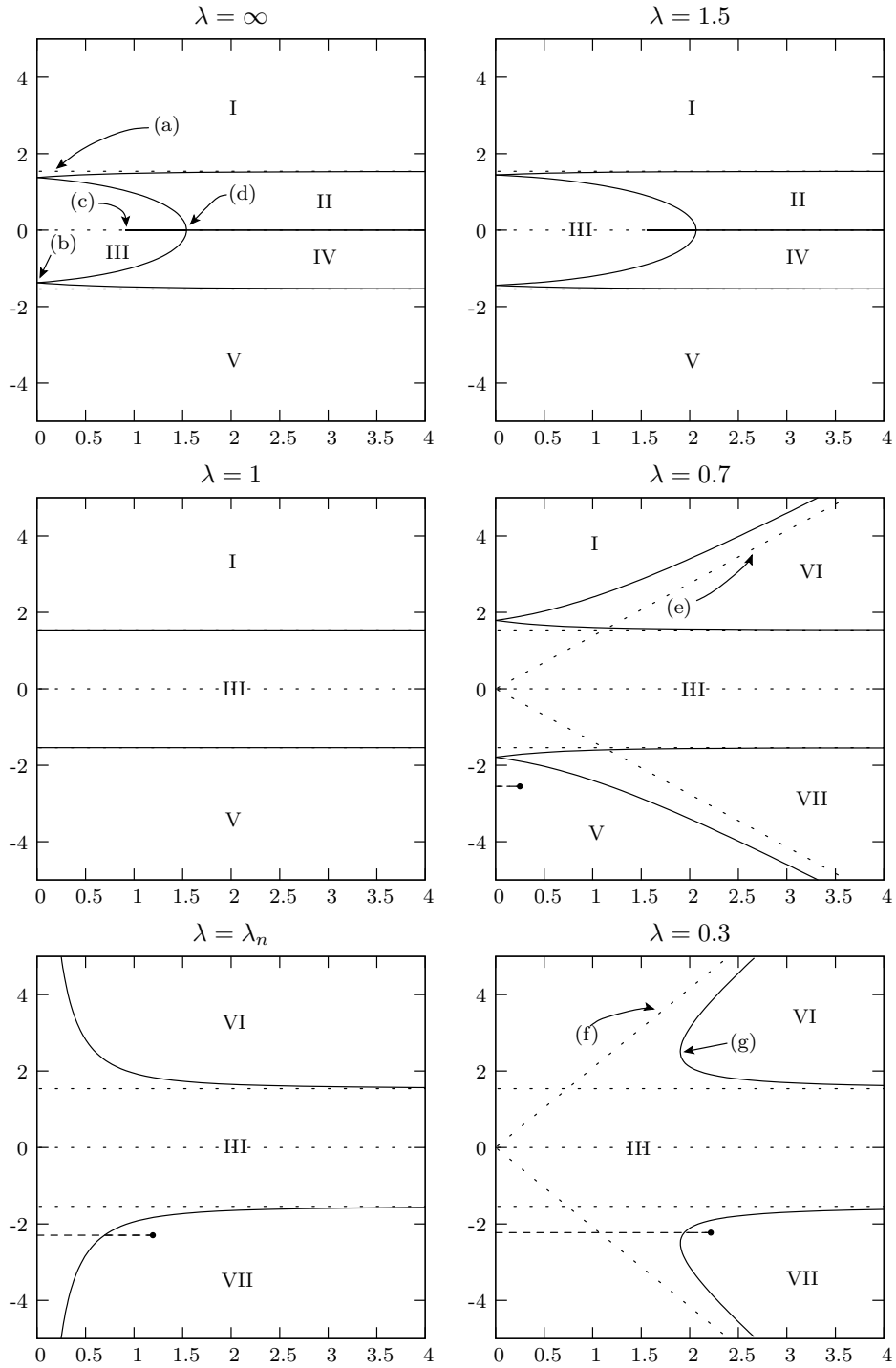


Figure 2: The anti-Stokes line $\text{Re}(\mu) = 0$ mapped into the Z plane for $U = 0.5$, giving $\lambda_n \approx 0.45$. The labelled points are displayed in table 1. The dashed line and filled circle are described in the text.

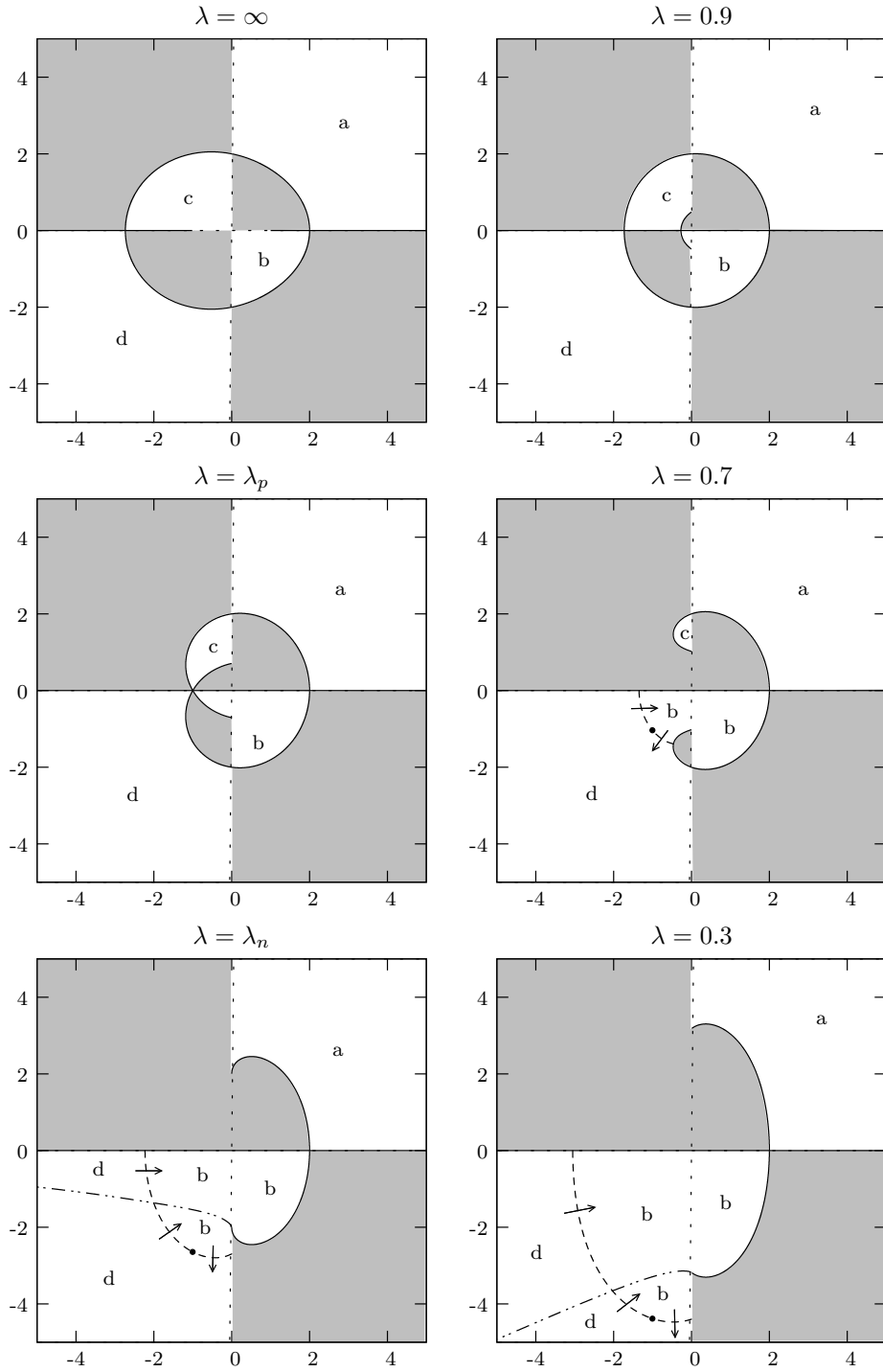


Figure 3: Schematic of the σ -plane showing the allowable locations of the surface modes a, b, c, and d. $\text{Re}(Z) = 0$ maps to the solid lines, with the shaded areas corresponding to $\text{Re}(Z) < 0$. The dashed line and filled circle are images of those in fig. 2. The boundary between regions III and VII maps to the dash-dot line. $U = 0.5$, giving $\lambda_p \approx 0.82$ and $\lambda_n \approx 0.45$.

$$\begin{aligned}
\text{(a)} \quad \text{Im}(Z) &= \frac{2U}{\beta^3} & \text{(b)} \quad Z &= \frac{2iU}{\beta^3\sqrt{1+\tau^2}} \\
\text{(c)} \quad Z &= \frac{U}{\beta^3} \frac{5+4\tau^2-3\sqrt{1+8\tau^2}}{\sqrt{2\sqrt{1+8\tau^2}-2-4\tau^2}} & \text{(d)} \quad Z &= \frac{U}{\beta^3\tau} \\
\text{(e)} \quad Z &= ((1-\tilde{\tau}^2)+2i\tilde{\tau})s & \text{(f)} \quad Z &= ((\tilde{\tau}^2-1)+2i\tilde{\tau})s \\
\text{(g)} \quad Z &= \frac{2U}{\beta^3\sqrt{\tilde{\tau}^2-1}} ((\tilde{\tau}^2-1)+i\sqrt{2\tilde{\tau}^2-1})
\end{aligned}$$

Table 1: Labelled points in fig. 2. $\tau = U\sqrt{1-\lambda^{-2}}$, and $\tilde{\tau} = U\sqrt{\lambda^{-2}-1}$ are used to simplify notation. Lines are parameterized by $s \in [0, \infty)$.

3.3 Position of surface modes

Fig. 3 shows a schematic of the allowable positions in the σ -plane for each of the four surface modes, labelled a, b, c, and d. The line $\text{Re}(Z) = 0$ is an important boundary, separating an energy absorbing duct wall ($\text{Re}(Z) > 0$) from an energy producing one ($\text{Re}(Z) < 0$). The trajectories of the surface modes in the σ -plane for $\text{Re}(Z) = 0$ give an egg-shaped contour for large enough λ , exactly as described in [1] where $\lambda = \infty$. It was pointed out in [1] that, since only energy absorbing duct boundaries are considered, no surface mode can cross this contour, and it turns out that this contour separates the individual surface modes from one another.

The egg-shaped contour remains qualitatively correct for all $\lambda > 1$, and indeed a very similar contour is found for λ just less than unity. At $\lambda = 1$ the two branches along the real σ axis meet at the origin, and for $\lambda < 1$ a new double root of (8) becomes present on the negative real σ axis. As λ approaches a critical value λ_p (determined below), the two double roots on the negative real σ axis coalesce, and for $\lambda < \lambda_p$ a topological change is seen, with $\text{Re}(Z) = 0$ now mapping to a mushroom-shaped contour. The critical value λ_n discovered earlier is seen to be the point at which the overhang on the base of the mushroom disappears, along with region V of the Z -plane which corresponds to the presence of the root inside the overhang (surface mode c).

As mentioned above, the quartic equation (8) for σ permits a double root for certain values of Z ; an obvious quadruple root is given by $\sigma = U^{-1}$, $Z = 0$ (corresponding to the right of the egg or the top of the mushroom). A value of Z leading to a double root in σ will be termed a *double root singularity*. A double root is indicated by the derivative (with respect to σ) of (8) being zero, in addition to (8) being satisfied. Requiring a zero derivative gives

$$\frac{\sigma}{2U} = \frac{1}{Z^2\beta^6}(1-U\sigma)^3.$$

Assuming $Z \neq 0$ and substituting the above into (8) to eliminate the Z dependence yields a quadratic equation for σ , giving solutions

$$\sigma_{\pm} = -\frac{1}{2U} \pm \sqrt{\frac{1}{4U^2} + 2\left(1 - \frac{1}{\lambda^2}\right)}, \quad Z_{\pm}^2 = \frac{2U}{\beta^6} \frac{(1-U\sigma_{\pm})^3}{\sigma_{\pm}},$$

the branch of Z_{\pm} being chosen such that $\text{Re}(\mu) > 0$. The coincidence of the double roots with $Z \neq 0$ occurs when $\sigma_+ = \sigma_-$, implying $\sigma = -1/(2U)$ and $\lambda = \lambda_p \equiv 1/\sqrt{1+U^{-2}/8}$. For $\lambda < \lambda_p$, Z_+ and Z_- move off the imaginary Z axis; one into the half plane $\text{Re}(Z) > 0$, the other into $\text{Re}(Z) < 0$.

The question of where in the σ -plane the surface modes exist, and which disappear when crossing an anti-Stokes line, may now be attended to. The existence of a double root singularity in the interior of the half plane $\text{Re}(Z) > 0$ complicates matters, since tracing modes as Z moves in a closed circle around such a singularity would show the b and d surface modes exchanging places. The position of the double root is shown as a filled circle in both fig. 2 and fig. 3 (the other double roots having either $\text{Re}(Z) < 0$ or $\text{Re}(\mu) < 0$). Also shown is a dashed line extending from the double root singularity to the imaginary Z axis, and its projection into the σ -plane. Taking this as a branch cut, the image of the branch cut may be used to separate the b and d modes. The arrows shown in fig. 3 show how the b and d modes would exchange places if Z were allowed to transition upwards across the branch cut. Above the dash-dot line corresponds to Z belonging to region III and only one of the b or d modes being present, while below

	a	b	c	d
I				
II	x			
III	x	1		2
IV	x	x	x	
V	x	x	x	x
VI		x		
VII	x	x		x

Table 2: Table showing which surface modes of fig. 3 are present for each region of fig. 2. Key: x) present. 1) present above a branch cut, or with no branch cut. 2) present only below a branch cut. blank) not present.

the dash-dot line corresponds to Z belonging to region VII and both b and d modes being present; it is in the latter case that the modes switch places.

With the branch cut as shown in fig. 2, the existence of each of the surface modes a, b, c, and d depends on which region Z is in, and is tabulated in table 2. The orientation of the branch cut is arbitrary; using a different branch cut would only change the labelling of some b surface modes to d, and vice versa. The branch cut used was chosen for simplicity.

3.4 Accuracy of the asymptotics

Fig. 4 shows the trajectories of modes in the k -plane as $\text{Im}(Z)$ is varied, with $\text{Re}(Z)$ fixed. Fig. 4(a) takes $\omega = 5$, $m = 1$, and $U = 0.5$, giving $\lambda \approx 5.8$, and corresponds to the top left diagram of fig. 7 in [1]. For such a relatively small value of ω the asymptotics do not show a perfect match, as the asymptotic results were obtained in the limit $\omega \rightarrow \infty$. In particular, both asymptotics switch from approximating one mode to approximating another, missing the fact that these modes are distinct. Nonetheless, both the current asymptotics and the asymptotics of [1] provide a good indication of the exact results. Fig. 4(a) also shows how the surface modes transition into duct modes, with the duct modes switching places to accommodate the new mode. This was discussed in [1], and since this behaviour is no different in the present case it is not discussed further here.

Fig. 4(b) uses $\omega = 31$, $m = 24$, and $U = 0.5$. These values were given in [2] as being realistic parameters for aeroengine intake noise at high power, and lead to $\lambda \approx 1.5$. The figure shows a very good agreement between the present asymptotic and exact results, while the predictions of [1] are noticeably less accurate. The other two surface modes are present, although not shown in fig. 4(b) due to the scale used, and are both accurately predicted by both asymptotic approximations.

4 Conclusion

An asymptotic dispersion relation for surface waves has been derived in the large m limit, and has been shown to generalize Rienstra's [1] high-frequency asymptotics to allow for arbitrary azimuthal wavenumbers m . The dimensionless number $\lambda = \omega/(m\beta)$ selects one of four surface-mode regimes, with $\lambda \rightarrow \infty$ corresponding to [1]. For $\lambda > 1$, the results of [1] are qualitatively correct, although for the aeroengine intake model suggested by [2] with $\lambda \approx 1.5$ the generalized asymptotics presented here provide a distinctly better approximation to the exact solution. For $\lambda_n < \lambda < 1$ different combinations of the four possible surface modes are available, where $\lambda_n \equiv 1/\sqrt{1+U^{-2}}$. For $\lambda < \lambda_n$ a maximum of three surface modes are possible, while as $\lambda \rightarrow 0$ only two of the surface modes survive. Thus for $m \gg \omega$ only two infinite series of surface modes are seen irrespective of the impedance Z (c.f. fig. 1). In addition, the egg separating the surface modes from one another in the k -plane changes in shape for $\lambda < 1$, and becomes a mushroom for $\lambda < \lambda_p$, where $\lambda_p \equiv 1/\sqrt{1+U^{-2}/8}$. This corresponds to a double root singularity moving off the imaginary Z axis, and a branch cut is necessary in order to maintain a consistent labelling of the surface modes. A horizontal branch cut in the Z -plane leads to a similar situation to the egg in the k -plane, with the missing side of the egg replaced by a branch cut.

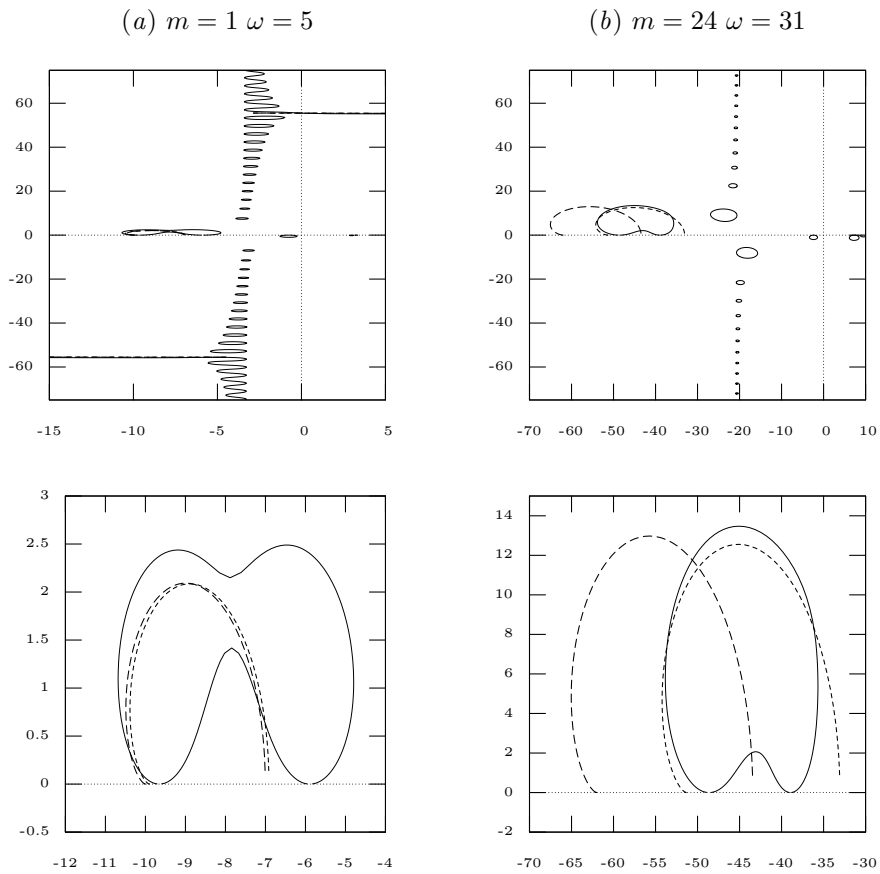


Figure 4: Comparison of current asymptotics (short dashed line), asymptotics of [1] (long dashed line) and exact results (solid line) for the axial wavenumber k . $\text{Re}(Z) = 3$, $\text{Im}(Z) \in (-\infty, \infty)$, and $U = 0.5$. The bottom diagrams show in more detail some of the modes of the upper plots.

McAlpine & Wright [2] proposed that at high power (with supersonic fan blade-tips) the dominant component of aeroengine fan noise is due to rotor-alone modes. For such a mode, Ω is the blade-tip Mach number and m is an integer multiple of the number of fan blades; the asymptotics presented here may therefore be thought of as a many-bladed approximation. In addition to rotor-alone modes, rotor-stator interaction modes result in a variety of values of m and ω , and our asymptotics also model such modes provided m is large; this may be thought of as a high-order-harmonic approximation. Finally, even if m is not significantly large, our asymptotics recover that of [1] which is valid in the limit $\omega \rightarrow \infty$, and therefore correspond to a high-frequency approximation. Our surface-mode asymptotics are therefore valid in a wide range of aeroacoustically relevant regimes.

Rienstra [1] went on to consider the stability of the surface-modes, and tentatively identified one of the four as an instability. The standard Briggs-Bers stability analysis is inapplicable in this case, since it turns out the temporal growth rate is unbounded for real wavenumbers. The alternative stability criterion used in [1] is an adaption of a method suggested by Crighton & Leppington without proof in [6], and its applicability to the current problem is uncertain. The present authors intend to address this in detail in a forthcoming paper.

Acknowledgements

The authors are very grateful to P. D. Metcalfe for numerous helpful discussions and suggestions. E. J. Brambley was supported by an EPSRC grant, and by Rolls-Royce plc under the University Gas Turbine Partnership research programme, and would like to thank both.

References

- [1] S. W. Rienstra, A classification of duct modes based on surface waves, *Wave Motion* **37** (2003) 119–135.
- [2] A. McAlpine, M. C. M. Wright, Acoustic scattering by a spliced turbofan inlet duct liner at supersonic fan speeds, *J. Sound Vib.* **292** (2006) 911–934.
- [3] M. E. Goldstein, Unsteady vortical and entropic distortions of potential flows round arbitrary obstacles, *J. Fluid Mech.* **89** (1978) 433–468.
- [4] M. K. Myers, On the acoustic boundary condition in the presence of flow, *J. Sound Vib.* **71**(3) (1980) 429–434.
- [5] M. Abramowitz, I. A. Stegun, *Handbook of Mathematical Functions* (Dover, 1974).
- [6] D. G. Crighton, F. G. Leppington, Radiation Properties of the Semi-Infinite Vortex Sheet: the Initial-Value Problem, *J. Fluid Mech.* **64**(2) (1974) 393–414.